

## Natural Carbonation of Alkali-Activated Fly Ash and Slag Pastes

Nedeljkovic, Marija; Zuo, Yibing; Arbi Ghanmi, Kamel; Ye, Guang

**DOI**

[10.1007/978-3-319-59471-2\\_253](https://doi.org/10.1007/978-3-319-59471-2_253)

**Publication date**

2018

**Document Version**

Final published version

**Published in**

High Tech Concrete: Where Technology and Engineering Meet

**Citation (APA)**

Nedeljkovic, M., Zuo, Y., Arbi Ghanmi, K., & Ye, G. (2018). Natural Carbonation of Alkali-Activated Fly Ash and Slag Pastes. In D. Hordijk, & M. Lukovic (Eds.), *High Tech Concrete: Where Technology and Engineering Meet: Proceedings of the 2017 fib Symposium, held in Maastricht, The Netherlands, June 12–14, 2017* (pp. 2213-2223) [https://doi.org/10.1007/978-3-319-59471-2\\_253](https://doi.org/10.1007/978-3-319-59471-2_253)

**Important note**

To cite this publication, please use the final published version (if applicable).  
Please check the document version above.

**Copyright**

Other than for strictly personal use, it is not permitted to download, forward or distribute the text or part of it, without the consent of the author(s) and/or copyright holder(s), unless the work is under an open content license such as Creative Commons.

**Takedown policy**

Please contact us and provide details if you believe this document breaches copyrights.  
We will remove access to the work immediately and investigate your claim.

# Natural Carbonation of Alkali-Activated Fly Ash and Slag Pastes

Marija Nedeljković<sup>1(✉)</sup>, Yibing Zuo<sup>1</sup>, Kamel Arbi<sup>1,2</sup>, and Guang Ye<sup>1</sup>

<sup>1</sup> Materials and Environment (Microlab), Faculty of Civil Engineering and Geosciences, Delft University of Technology, P.O. Box 5048, 2600 GA Delft, The Netherlands

{M. Nedeljkovic, Y. Zuo, K. Arbi, G. Ye}@tudelft.nl

<sup>2</sup> Delta Concrete Consult BV & Nebest Adviesgroep, Mrconiweg 2, 4131 PD Vianen, The Netherlands

Kamel.Arbi@deltaconcreteconsult.nl

**Abstract.** The carbonation-induced degradation in alkali-activated materials (AAMs) is unknown. This is due to the current level of understanding of the carbonation mechanism in accelerated conditions, whereas the results from the long-term performance of AAMs in service are not available.

In this paper, the natural laboratory carbonation of alkali-activated fly ash (FA) and blast furnace slag (BFS)-based pastes was studied. The aim of experiments was to investigate the influence of the binder composition on the carbonation mechanism. The microscope techniques, i.e. polarization, fluorescent and Environmental Scanning Electron Microscope (ESEM) enabled the identification of the carbonation front and local defects due to carbonation, such as microcracks, and pore structure changes. The pH of the simulated pore solution in carbonated and noncarbonated samples was analyzed. The pore structures after carbonation were characterized in terms of capillary and gel pores by Mercury Intrusion Porosimetry (MIP) and nitrogen sorption. The effect of the change in the porosity on the mechanical properties was examined by Nanoindentation tests.

Results show that the natural carbonation did not reduce the alkalinity of the pore solution to below the pH 9. The pH was kept above 10.5 in all the mixtures. The samples with 50 wt% and less BFS content, were uniformly carbonated. The increase of the total porosity in those samples has been attributed to the simultaneous effect of the carbonation and drying shrinkage of the pastes. The change in the porosity for a consequence has a reduction in the modulus of elasticity. The samples containing more than 50 wt% of BFS were fully resistant to carbonation or carbonation was induced along the cracks as observed from the microscopic analysis.

**Keywords:** AAMs · Natural carbonation · Durability · Pore structure

## 1 Introduction

AAMs have excellent mechanical properties, chemical resistance, and high thermal stability compared to the Ordinary Portland cement (OPC)-based materials (Provis 2014). They are more sustainable due to the use of industrial by-products instead of the natural

resources for their composition. Therefore, AAMs are emerging as a viable alternatives to the OPC. However, the durability of AAMs is still unknown, which limits their application in the engineering practice. For instance, understanding of the carbonation-induced degradation in AAMs in service is essential, since it is the process that causes both, the chemical and physical changes of the material properties (Arbi et al. 2016).

In the OPC-based materials, carbonation is known as a chemical reaction between carbon acid formed in the pore solution, calcium hydroxide ( $\text{Ca}(\text{OH})_2$ ) and hydrated calcium silicate (C-S-H). It results primarily in the reduction of the pH, which is mainly controlled by the content of  $\text{Ca}(\text{OH})_2$  (Morandeu et al. 2014). However, the  $\text{Ca}(\text{OH})_2$  is usually not formed in AAMs (Oh et al. 2010). Therefore, the pH of the pore solution in AAMs depends on the concentration of alkalis that are used in the alkaline activator and contained in a raw materials. The principal binding phase that can be carbonated in FA and BFS-based AAMs is calcium aluminosilicate C-A-S-H gel (Bernal et al. 2013). Regarding material properties, carbonation progress will be dependent on the binder chemical composition and the pore structure (size distribution, connectivity, and tortuosity). The mechanism will be certainly different to that reported in OPC-based materials due to the difference in the primary reaction products between OPC and AAMs, and owing to the more dense microstructure formation in the blended FA and BFS-based AAMs. Furthermore, the gel pores are identified to be the main contributor to the total pore volume in AAMs, when 50 wt% BFS or more is used in the mixture composition (Nedeljkovic et al. 2016). Due to the significant decrease of the volume of capillary pores in those systems (Nedeljkovic et al. 2016), carbonation is assumed not to be the diffusion driven process such as reported in the OPC-based materials (Morandeu et al. 2014). Instead, the chemical reactions and diffusion are believed to be the simultaneous drivers for the carbonation in AAMs. The kinetics of the chemical reactions will be contingent on the chemical composition of the raw materials, which governs the resultant gel composition, porosity, permeability, and resistance to the carbonation (Bernal et al. 2013). The effects of the carbonation chemical reactions on the pore structure and the mechanical properties of the AAMs are not reported yet.

Therefore, the aim of this study was to evaluate the changes undergone by the alkali-activated FA and BFS pastes due to the natural laboratory carbonation, with 55% RH, 20 °C. The specific objectives were to investigate the effect of the carbonation by the investigation of the pore structure, modulus of elasticity, hardness of the samples, and the alkalinity of the pore solution. The microscopy tests were carried out on the samples after the exposure to investigate the carbonation front and observe microstructural changes. The alkalinity of the pore solution was measured by the suspension method. The MIP, nitrogen sorption and Nanoindentation technique were used to examine the pore structure and the mechanical properties.

## 2 Materials and Methods

### 2.1 Materials and Sample Preparation

The precursors used in this study were FA and BFS. The chemical compositions of the precursors were determined by XRF (Table 1). The alkaline activator was prepared by

mixing two solutions, the sodium hydroxide and sodium silicate. After mixing, the activator was cooled down to room temperature prior to the preparation of the pastes. The liquid to binder mass ratio was 0.5. Pastes were produced with the following ratios of FA and BFS, 100:0, 70:30, 50:50, 30:70, 0:100 wt%, named S0, S30, S50, S70, S100. The precursors were dry-mixed for 3 min and then mixed with the activator. The pastes were cast in the cylinder moulds of  $54 \times 100 \text{ mm}^2$ . The samples were sealed cured for 28 days. After 28 days of curing in fog room samples were removed from cylinder moulds to the indoors laboratory conditions at  $20 \text{ }^\circ\text{C}$  and 55% RH for 1 year. On the other hand, reference samples were kept in a sealed conditions without  $\text{CO}_2$  until the characterization was carried out. The representative samples prior to microscopic examination are shown in the Fig. 1.



**Fig. 1.** Cross sections of the representative samples after natural carbonation of 1 year- the outer (carbonated zone) and the inner (noncarbonated zone), reference samples are of the smaller diameter, placed beneath exposed samples.

**Table 1.** Chemical compositions of FA and BFS measured by X-ray fluorescence

	$\text{SiO}_2$	$\text{Al}_2\text{O}_3$	$\text{CaO}$	$\text{MgOO}$	$\text{Fe}_2\text{O}_3$	$\text{SO}_3$	$\text{Na}_2\text{OO}$	$\text{K}_2\text{OO}$	$\text{TiO}_2$	$\text{P}_2\text{O}_5$	L.O.I.
FA	54.28	23.32	4.23	1.62	8.01	0.64	0.85	1.97	1.23	0.54	3.37
BFS	34.40	11.53	39.17	7.81	1.42	1.6	0.23	0.58	–	–	1.15

## 2.2 Methods

The carbonation depth was measured by phenolphthalein indicator. For the pH measurements, it was not possible to extract liquid pore solution due to the density of the samples. Therefore, the analyses were carried out on the simulated pore solution. The simulated pore-solution was prepared by dissolving 1 g of powdered sample in 10 ml of de-ionized water. The suspension was maintained during 1 h at ambient temperature, after which the pH was measured by a standard color chart and pH meter 827 Metrohm. Polarization, fluorescence and ESEM were used to observe microstructural changes. For this purpose, thin sections were prepared by first sawing small prisms from the samples. The dimensions of the prisms were  $50 \text{ mm} \times 30 \text{ mm}$ , with a thickness of

about 10 mm. The sawn prisms were impregnated under vacuum with an epoxy resin containing a fluorescent dye. The thickness of the final thin sections was around 30  $\mu\text{m}$  to provide sufficient light transmission for microscopic analysis. Porosity and pore-size distribution were investigated by two methods, MIP and nitrogen sorption test, following the sample preparation procedure as reported in (Ye 2003). The sharp peaks that were found in the pore size distributions curves, corresponding to the threshold (critical) pore diameter were determined according to Katz and Thompson (1986). The microstructure of the carbonated and noncarbonated samples was examined mechanically by Agilent Nano Indenter G200 with a diamond Berkovich tip, while the samples were prepared according to the procedure described in (Lukovic 2016).

### 3 Results and Discussion

#### 3.1 Carbonation Depth and Simulated Pore Solution

The carbonation depth was determined by the phenolphthalein indicator (Fig. 2) and Polarization microscope (Figs. 5 and 6), which is further discussed in Sect. 3.2. From measured carbonation depths (Fig. 3) it can be seen that mixtures with 50 wt% and less BFS carbonate faster. The pH was tested in the simulated pore-solution of the three states of material for each mixture, carbonated edge, carbonated middle and reference sample after 28 days of curing and after 1 year of carbonation (Fig. 4).

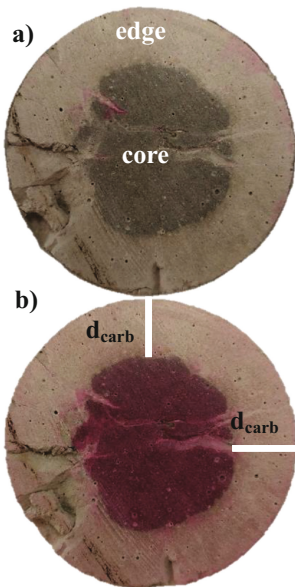


**Fig. 2.** (a) Photo of the sample S50 before and (b) after spraying the pH indicator.

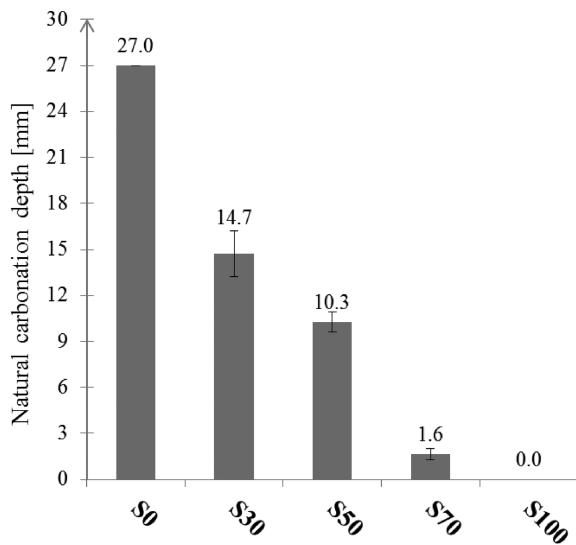


**Fig. 3.** Natural carbonation depth (12 months exposure to ambient laboratory environment) of alkali-activated pastes ( $\phi = 27$  mm) as a function of the slag content in the paste.

For reference samples at 28 days, the pH is maintained around 13.5 for all the mixtures (Fig. 4). After 1 year of curing, the pH drops for 2 units, suggesting that OH<sup>-</sup> ions were consumed by alkaline activation. On the other hand, the samples that are noted as carbonated edge have a pH that is reduced due to natural carbonation, but not below 10.5.

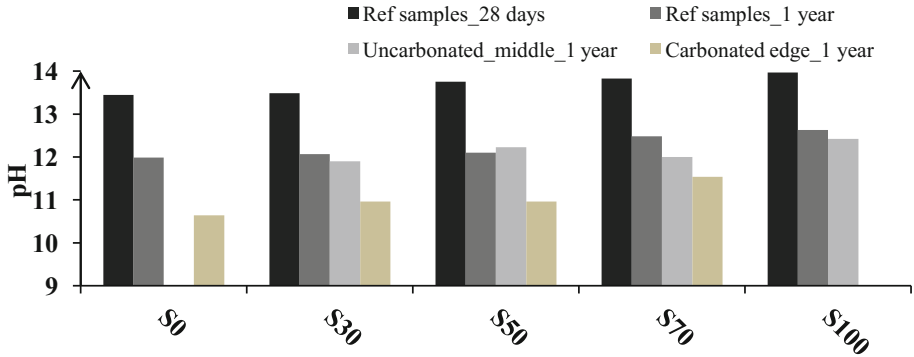


Fig. 4. The pH of the simulated-pore solutions (12 months exposure to the ambient laboratory environment) of alkali-activated pastes ( $\phi = 27$  mm) as a function of the slag content in the paste (samples from Fig. 1).

### 3.2 Microscopic Study

As a result of differences in the FA replacement by BFS, each paste has presented a unique microstructural pattern including voids, defects, and carbonation front according to the fluorescent microscopic study (Fig. 6). One of the paste, S50 which demonstrated the most different pattern was selected for further examination by Polarization, Fluorescent and ESEM microscopes (Figs. 5 and 8).

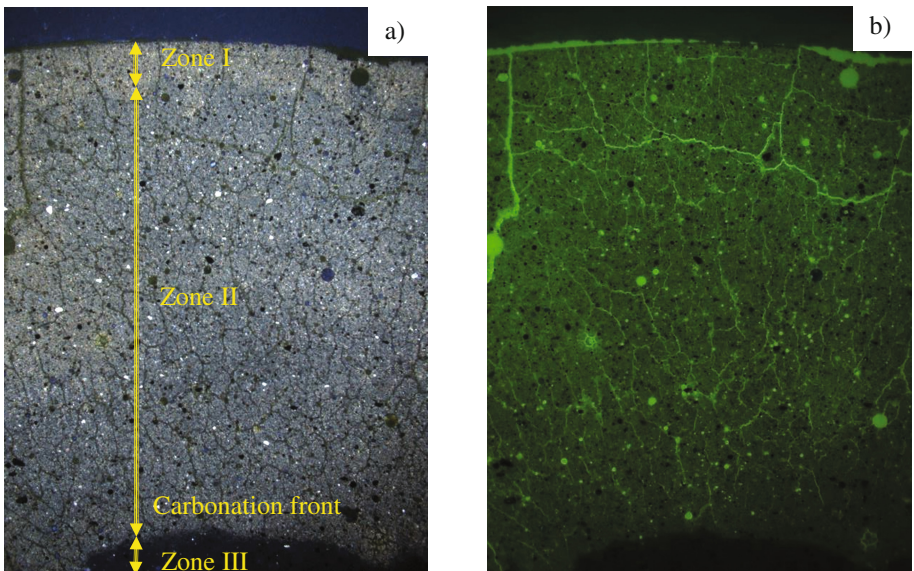
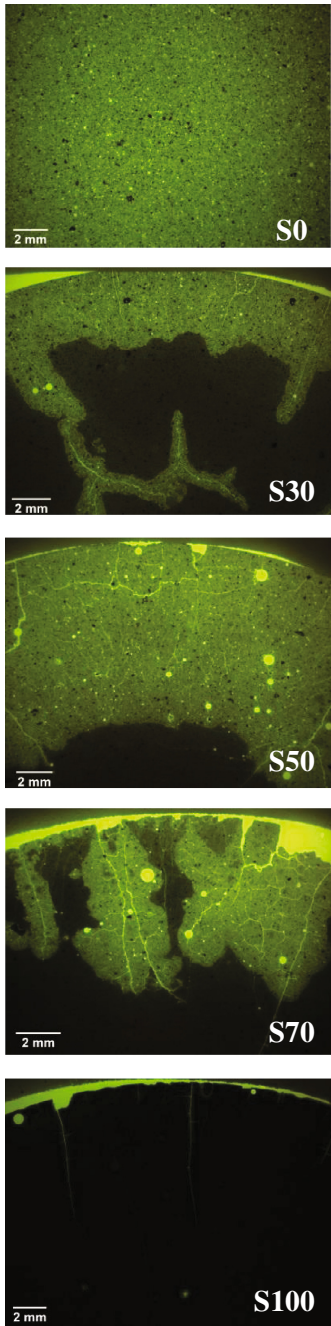


Fig. 5. Photo of S50 thin section under (a) polarization, and (b) fluorescent light



**Fig. 6.** Fluorescent microscopy on the cross-sections of five different pastes after 1 year of the natural carbonation.

The low magnification images obtained by fluorescent microscope are shown in Fig. 6. A general pattern in each of the cross-sections of carbonated samples can be observed. The existing defects can be then clearly seen, due to the impregnation with resin. The paste S0 demonstrated continuous carbonation where the resin uniformly filled the section indicating the high porosity of the sample. No defects such as voids and microcracks can be observed in S0. In the sample S30, continuous cracks can be observed along the cross-section. These cracks are most likely induced by the drying shrinkage during curing and carbonation exposure of the samples. They initiate from the top surface and progress toward the core of the sample. The S50 sample also demonstrated uniform carbonation depth (Fig. 5a, b). In this sample, noncarbonated zone did not show any defects or voids. Conversely, in carbonated zone the entire section presented extensive cracking. A degraded area was clearly separated by a front line (carbonation front) from the noncarbonated zone. S70 contains multiple cracks perpendicular to the edge of the sample which are originated from the edge towards the centre of the sample. In noncarbonated zone the cracks were not identified. According to this observation, the carbonation in S70 is mainly induced in the vicinity of the cracks. Carbonation depth of the surface layer of S70 is smaller than the carbonation depth induced left or right from the axe of the crack. This can be explained by the difference in moisture content at the top of the surface and in depth of the sample. Due to dry top surface, carbonation reaction will be restricted by no presence of the moisture or its very low content (less than 50% RH), whereas in the crack RH is higher and thus carbonation can occur faster. S100 paste was found to be highly resistant to carbonation owing to its highly dense microstructure. Regarding S50, beside fluorescent microscopic analysis (Fig. 5 b), the cross section was also observed under Polarization light. Three zones can be distinguished in the thin section (Fig. 5a),

1. Zone I (outer) - exposed paste surface fully degraded,
2. Zone II (middle) - blue zone with carbonates deposited,
3. Zone III (inner) - non-degraded.

The cracking in the degraded zone can be attributed to the drying shrinkage or to the one or more chemical transformations linked to the alteration of the phases due to carbonation, most likely decalcification of the gel. Most cracks are limited to the zones I and II. The Zone I is a zone with the most deterioration confined to near the outer surface. In addition, polarized light microscope was used to detect the front between carbonated and noncarbonated zones. In the thin section, the carbonation front is assessed by the presence of calcium carbonate crystals (white colour of crystals in the carbonated zone, Fig. 7). In terms of the optical properties, calcium carbonate is extremely birefringent, so it can be easily detected. The ESEM image (Fig. 8) clearly shows carbonation shrinkage in the S50 paste after 1 year of natural carbonation. The carbonation of the C-A-S-H gel is involving both the decalcification of the gel and polymerization of silicate chain that stays behind. The structural rearrangement of the partially carbonated gel will result in the overlapping between silicate chains, which creates more small gel pores and leads to the gel shrinkage. When 30 wt% or 50 wt% of BFS is used in the mixture design, carbonation shrinkage is larger. This is supported by the nitrogen adsorption measurement of the increase of the gel surface area (Table 3). S70 was less degraded since this paste is denser, compared to S50. Drying shrinkage also contributed to the appearance of the cracks (Fig. 8.), since the laboratory RH ( $\sim 55\%$ ) was very low.

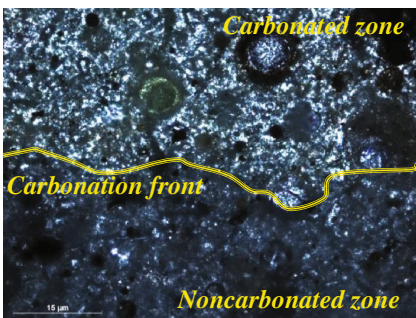


**Fig. 7.** Polarization micrograph of clearly distinguished uncarbonated and carbonated zone in the paste S50.

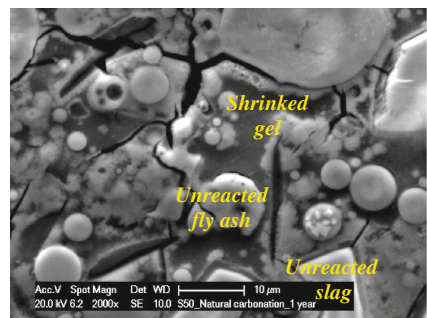


**Fig. 8.** ESEM micrograph of degraded zone microstructure in carbonated zone of the paste S50.

### 3.3 Effect of the Carbonation on the Porosity Development by MIP and Nitrogen Sorption Test

Pore size measurements were carried out in the pastes exposed to natural carbonation and reference pastes after 1 year. The MIP results for all the mixtures and the main pore structure characteristics are presented in Table 2, while cumulative intruded pore

volume curves and corresponding pore size distributions obtained for carbonated and reference samples of the paste S50 are presented in the Fig. 9. The physical meaning of a threshold pore diameters reported in Table 2 is that the pores whose diameter is greater than this diameter cannot form connected path throughout the sample (Ye 2003). It should be noted that the threshold pore diameter was not possible to be determined for reference samples and for some of carbonated samples (S70, S100), suggesting very dense microstructures. The MIP tests for the samples after 1 year of the exposure, have shown no significant change in the volume of capillary pores, compared to the reference samples (no carbonation).

**Table 2.** Capillary pore structure properties by MIP

Mixtures	Threshold pore access diameter (μm) REF	Threshold pore access diameter (μm) CARB	Total porosity [%] by volume REF	Total porosity [%] by volume CARB
S0	0.120	0.134	43.72	30.41
S30	–	0.028	26.04	26.22
S50	–	0.018	9.404	17.09
S70	–	–	6.538	9.66
S100	–	–	3.57	3.38

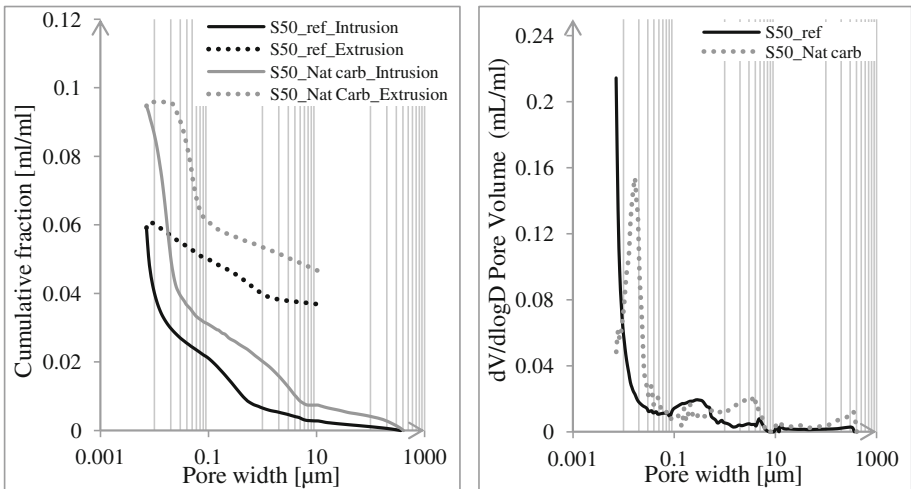


**Fig. 9.** Capillary pore volume and pore size distribution of paste S50 (reference and carbonated material)

The major change is in BET surface area, i.e. increase of the gel pores surfaces (Table 3). For instance, the results have shown that the carbonated zone in the S50 sample has more than 20 times higher BET surface area compared to the reference sample. This increase cannot be only attributed due to the widening of the gel pores

**Table 3.** Gel pore structure properties by Nitrogen adsorption, evolution of the BET surface area

Mixtures	Threshold pore access diameter (nm) REF	Threshold pore access diameter (nm) CARB	BET surface area [m <sup>2</sup> /g] REF	BET surface area [m <sup>2</sup> /g] CARB
S0	8.38	7.84	15.85	6.71
S30	5.52	7.29	2.58	27.91
S50	6.16	7.47	1.57	34.89
S70	6.57	6.25	0.88	25.1
S100	6.01	–	0.78	0.25

because of the chemical alterations of the gel under carbonation. The microcracks that belongs to the carbonated zone (Fig. 5) are also contributing to the increase in the total porosity.

### 3.4 Effect of the Carbonation on the Mechanical Properties by Nano-Indentation

Carbonation causes reduction in the modulus of elasticity in the 21-45 GPa range (S50 sample), where values corresponds to the modulus of elasticity of the main binding phases (Fig. 10). The ESEM image (Fig. 8) showed that the gel shrinkage and increase in the gel pore surface area (Table 3) are the possible reasons for the reduction in the modulus of elasticity. Nevertheless, it is also assumed that the structural change of the C-A-S-H gel by the decalcification and polymerization of silica chains due to carbonation (Bernal et al. 2013) contribute to the drop in modulus of elasticity. This is a reason for further research in this direction. On the other hand, the hardness of the carbonated zone did not significantly change compared to the noncarbonated zone.

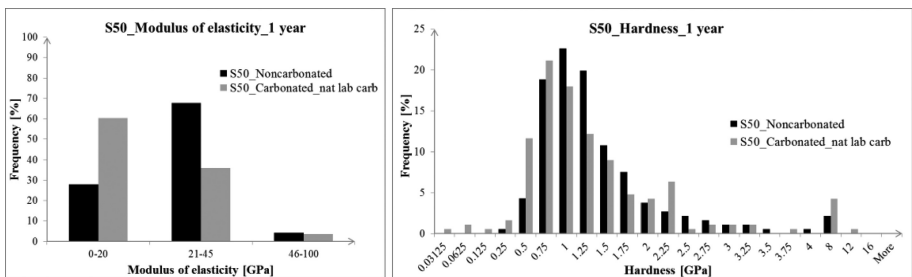


**Fig. 10.** Nano-indentation tests in the carbonated and noncarbonated S50 paste (left: modulus of elasticity, right: hardness).

## 4 Conclusions

The pH of all the mixtures after carbonation was above the pH 9, which is reported as a threshold value for an initiation of the carbonation induced reinforcement corrosion in the OPC-based binders. Therefore, corrosion of the reinforcement in the alkali-activated mixtures is expected not to be a concern regarding its initiation by the carbonation. The main difference in the pore size distribution was observed in the level of the gel pore sizes in the mixtures with 50 wt% and less BFS content, whereas the change in the volume and size of the capillary pores was minor. This is an indication for the gel degradation induced by the carbonation but also due to the drying regime as observed from the microscopic study. The consequences are the gel shrinkage, followed by the microcracking of the sample, which ultimately leads to the decrease in the elasticity of the matrix. The modulus of elasticity decreased by half in the mixture S50, whereas no significant change of the modulus of elasticity was found in the mixtures with more than 50 wt% of BFS. If the mixtures with more than 50 wt% are used, such as 70 wt% or 100 wt% of BFS, carbonation is not experienced due to their highly dense and compact microstructures. The hardness of all the mixtures was not affected.

**Acknowledgement.** This research was carried out under the project S81.1.13498 in the framework of the Partnership Program of the Materials innovation institute M2i ([www.m2i.nl](http://www.m2i.nl)) and the Technology Foundation STW ([www.stw.nl](http://www.stw.nl)), which is part of the Netherlands Organisation for Scientific Research ([www.nwo.nl](http://www.nwo.nl)). The authors thank Oguzhan Copuroglu for his help with the microscopic study.

## References

- Arbi, K., Nedeljkovic, M., Zuo, Y., Ye, G.: A review on the durability of alkali-activated fly ash/slag systems: advances, issues, and perspectives. *Ind. Eng. Chem. Res.* **55**(19), 5439–5453 (2016)
- Bernal, S.A., Provis, J.L., Walkley, B., San Nicolas, R., Gehman, J.D., Brice, D.G., van Deventer, J.S.: Gel nanostructure in alkali-activated binders based on slag and fly ash, and effects of accelerated carbonation. *Cem. Concr. Res.* **53**, 127–144 (2013)
- Katz, A.J., Thompson, A.H.: Quantitative prediction of permeability in porous rock. *Phys. Rev. B* **34**(11), 8179 (1986)
- Lukovic, M.: Influence of interface and strain hardening cementitious composite (SHCC) properties on the performance of concrete repairs. PhD thesis, Delft University of Technology, The Netherlands (2016)
- Morandau, A., Thiery, M., Dangla, P.: Investigation of the carbonation mechanism of CH and CSH in terms of kinetics, microstructure changes and moisture properties. *Cem. Concr. Res.* **56**, 153–170 (2014)
- Nedeljkovic, M., Arbi, K., Zuo, Y., Ye, G.: Physical properties and pore solution analysis of alkali-activated fly ash-slag pastes. In: 2016 Proceedings pro113: International RILEM Conference Materials Systems and Structures in Civil Engineering 2016 (MSSCE 2016) on Concrete with Supplementary Cementitious Materials (2016)

- Oh, J.E., Monteiro, P.J., Jun, S.S., Choi, S., Clark, S.M.: The evolution of strength and crystalline phases for alkali-activated ground blast furnace slag and fly ash-based geopolymers. *Cem. Concr. Res.* **40**(2), 189–196 (2010)
- Provis, J.L.: Geopolymers and other alkali activated materials: why, how, and what? *Mater. Struct.* **47**(1–2), 11–25 (2014)
- Ye, G.: The microstructure and permeability of cementitious materials. PhD thesis, Delft University of Technology, The Netherlands (2003)